Structure-Based Engineering of Internal Cavities in Coiled-Coil Peptides[†,‡]

Maneesh K. Yadav, James E. Redman, Luke J. Leman, Julietta M. Alvarez-Gutiérrez, Yanming Zhang, C. David Stout, and M. Reza Ghadiri*

Departments of Chemistry and Molecular Biology and The Skaggs Institute of Chemical Biology, The Scripps Research Institute, 10550 North Torrey Pines Road, La Jolla, California 92037

Received April 22, 2005; Revised Manuscript Received May 26, 2005

ABSTRACT: Cavities and clefts are frequently important sites of interaction between natural enzymes or receptors and their corresponding substrate or ligand molecules and exemplify the types of molecular surfaces that would facilitate engineering of artificial catalysts and receptors. Even so, structural characterizations of designed cavities are rare. To address this issue, we performed a systematic study of the structural effects of single-amino acid substitutions within the hydrophobic cores of tetrameric coiled-coil peptides. Peptides containing single glycine, serine, alanine, or threonine amino acid substitutions at the buried L9, L16, L23, and I26 hydrophobic core positions of a GCN4-based sequence were synthesized and studied by solution-phase and crystallographic techniques. All peptides adopt the expected tetrameric state and contain tunnels or internal cavities ranging in size from 80 to 370 Å^3. Two closely related sequences containing an L16G substitution, one of which adopts an antiparallel configuration and one of which adopts a parallel configuration, illustrate that cavities of different volumes and shapes can be engineered from identical core substitutions. Finally, we demonstrate that two of the peptides (L9G and L9A) bind the small molecule iodobenzene when present during crystallization, leaving the general peptide quaternary structure intact but altering the local peptide conformation and certain superhelical parameters. These high-resolution descriptions of varied molecular surfaces within solvent-occluded internal cavities illustrate the breadth of design space available in even closely related peptides and offer valuable models for the engineering of de novo helical proteins.

A significant challenge frustrating the de novo design of functional molecules is that of precisely constructing molecular surfaces able to suitably participate in desired molecular recognition events. Internal cavities, relatively buried clefts, and tunnels are frequently important sites of interaction between natural enzymes or receptors and their corresponding substrate or ligand molecules, and the ability to engineer such surfaces would facilitate the successful design of highly selective artificial catalysts and receptors. Mutagenesis of natural proteins to create or alter internal cavities has been used for purposes such as redesigning enzyme specificities, creating novel binding sites, and studying protein stability (*1*−*12*), but despite the diverse roles of natural cavities in biology, high-resolution structural investigations of model cavities in the aqueous milieu are rare. We believe studying designed cavities within synthetic peptides may provide models for understanding natural binding sites as well as designing novel receptors or biocatalysts.

[†] We thank the National Institutes of Health for financial support (Grant GM52190). J.E.R., J.M.A.-G., and L.J.L. thank the Wellcome Trust (061454/Z/00/Z), the Spanish MCYT, and NSF, respectively, for fellowships.

[‡] Coordinates have been deposited in the RCSB Protein Data Bank: entry 1UO2 for GCN4-pLI, entry 1UO3 for L9G, entry 1UNU for L9S, entry 1UNT for L9A, entry 1UNV for L9T, entry 1UO4 for L9G+IB, entry 1UO5 for L9A+IB, entry 1UNW for L23G, entry 1UNX for L23S, entry 1UNY for I26G, entry 1UNZ for I26S, entry 1UN0 for I26A, entry 1UN1 for I26T, entry 1W5I for L16G E20C, and entry 2BNI for L16G E20C Y17H.

* To whom correspondence should be addressed. Phone: (858) 784-2700. Fax: (858) 784-2798. E-mail: ghadiri@scripps.edu.

The most-studied motif in de novo protein engineering is the coiled coil (*13*), a naturally derived peptide assembly composed of two or more α-helices wrapped around each other to bury a hydrophobic core. The homotetrameric GCN4-pLI coiled coil (*14*) is an attractive scaffold for engineering cavities because (a) it is amenable to backbone and amino acid substitution without significant perturbation of the overall structure (*15*, *16*), presumably because it is one of the most stable reported GCN4-derived peptides, (b) its crystal structure is known (*14*), allowing structure-based design of internal cavities, and (c) the interhelical distance is greater in the tetramer than in other naturally derived dimeric or trimeric coiled coils (*14*), allowing the formation of large internal cavities.

Most previous work involving hydrophobic core substitutions in coiled-coil peptides has focused on the structural effects of buried polar residues (especially Asn and Gln) in specifying the oligomerization state or strand orientation (*17*, *18*), although several reports of observed or designed cavities have also been published. Benzene binding in the designed cavity of a coiled-coil trimer was found to control the peptide's configuration (*19*, *20*), and internal cavities were more recently described in the crystal structures of peptides containing Ser or Thr core substitutions (*21*). Apart from these examples, however, engineered cavities in coiled-coil systems have gone without high-resolution characterization. A template-assembled trimeric bundle containing Leu → Ala core substitutions was shown to bind a fluorescent ligand (*22*), and similarly, tri- and tetrameric bundles containing

10.1021/bi050742a CCC: $30.25
Published on Web 06/23/2005

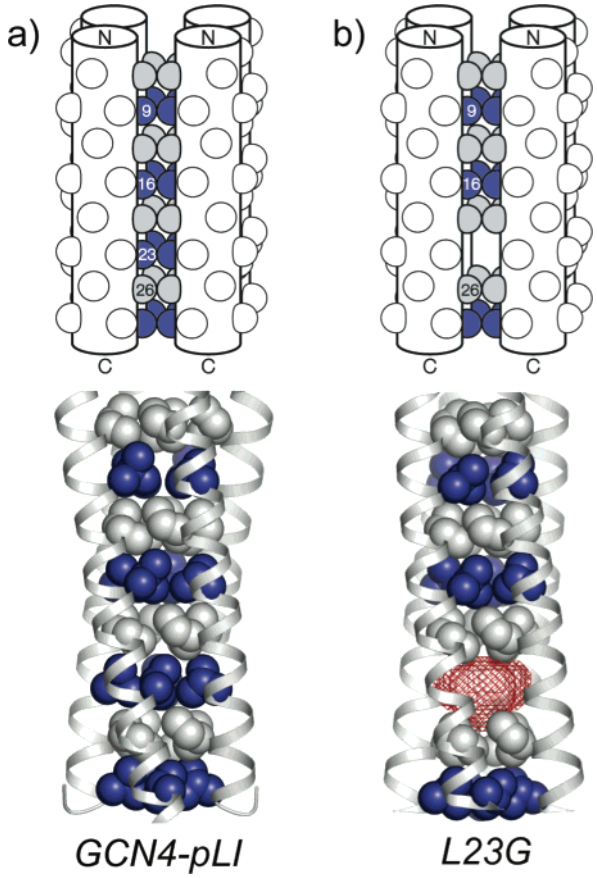

FIGURE 1: Engineering internal cavities in tetrameric coiled coils. Upon assembly of the noncovalent tetramer, the spatial localization of one large-to-small amino acid substitution from each strand creates a buried cavity. Representative schematic diagrams (top) and crystal structures (bottom) are shown for (a) GCN4-pLI and (b) the L23G variant, emphasizing hydrophobic core *a* position Leu (blue) and *d* position Ile (gray) residues. The sites of large-to-small core substitutions described in this paper are numbered in the schematic diagrams. In the L23G crystal structure, the 280 Å^3 cavity (probe-occupied volume using a probe with a radius of 1.4 Å) is colored red.

core substitutions have been show to bind a volatile anesthetic (*23*−*26*). The prevention of cavity formation, or steric matching, has recently been described as a means of controlling quaternary structure in trimeric peptide assemblies (*27*, *28*), whereas pairs of Ala core substitutions have been shown to be capable of controlling the parallel/antiparallel configuration and the aggregation state of coiled-coil peptides (*29*, *30*), reportedly due to thermodynamic preferences for avoiding large internal cavities. These several examples illustrate not only the utility of cavities in protein engineering but also the need for structural characterizations of such surfaces to allow us to more fully understand the means by which they alter protein folding and function.

We initially set out to perform a systematic study of the structural effects of single-amino acid substitutions within the hydrophobic core of parallel coiled-coil tetramers, with the specific goal of generating discrete internal cavities by replacing bulky hydrophobic residues at core *a* and *d* positions with smaller amino acids (Figure 1). After subsequently coming to appreciate the plasticity of the scaffold to amino acid substitution, and considering the recently reported structural characterization of antiparallel tetrameric coiled coils (*31*), we expanded our initial goal to include

Table 1: Peptide Sequences and Nomenclature

Peptide	Sequence
GCN4-pLI	Ac-R-MKQIEDK-LEEILSK-LYHIENE-LARIKKL-LGER-OH
L9G	Ac-R-MKQIEDK-**G**EEILSK-LYHIENE-LARIKKL-LGER-OH
L9S	Ac-R-MKQIEDK-**S**EEILSK-LYHIENE-LARIKKL-LGER-OH
L9A	Ac-R-MKQIEDK-**A**EEILSK-LYHIENE-LARIKKL-LGER-OH
L9T	Ac-R-MKQIEDK-**T**EEILSK-LYHIENE-LARIKKL-LGER-OH
L16G E20C	Ac-R-MKQIEDK-LEEILSK-**G**YHIC̲NE-LARIKKL-LGER-OH
L16G E20C Y17H	ABA[a]-R-MKQIEDK-LEEILSK-**G**HHIC̲NE-LARIKKL-LGER-OH
L23G	Ac-R-MKQIEDK-LEEILSK-LYHIENE-**G**ARIKKL-LGER-OH
L23S	Ac-R-MKQIEDK-LEEILSK-LYHIENE-**S**ARIKKL-LGER-OH
L23A	Ac-R-MKQIEDK-LEEILSK-LYHIENE-**A**ARIKKL-LGER-OH
L23T	Ac-R-MKQIEDK-LEEILSK-LYHIENE-**T**ARIKKL-LGER-OH
I26G	Ac-R-MKQIEDK-LEEILSK-LYHIENE-LAR**G**KKL-LGER-OH
I26S	Ac-R-MKQIEDK-LEEILSK-LYHIENE-LAR**S**KKL-LGER-OH
I26A	Ac-R-MKQIEDK-LEEILSK-LYHIENE-LAR**A**KKL-LGER-OH
I26T	Ac-R-MKQIEDK-LEEILSK-LYHIENE-LAR**T**KKL-LGER-OH

[a] ABA is acetamidobenzoic acid.

investigation of internal cavities within peptides likely to adopt the antiparallel configuration. Along with solution-phase biophysical data, we report here crystal structures of one antiparallel and 11 parallel GCN4-pLI variants containing tunnels or internal cavities ranging in volume from 80 to 370 Å^3 (total volume occupied by a probe with a radius of 1.4 Å), a subset of which (L9G and L9A) bind iodobenzene in the crystalline state with conformational changes reminiscent of induced fit binding events in natural receptors. These high-resolution snapshots of varied molecular surfaces in peptides adopting nearly identical quaternary structures illustrate the wide breadth of design space available in even closely related peptides and may offer valuable models for the engineering of de novo helical proteins.

MATERIALS AND METHODS

Peptide Sequence and Nomenclature. The sequences of the GCN4-pLI variants described herein are listed in Table 1. The peptides are named by their core substitutions (for example, the variant containing the Leu → Ala substitution at position 9 is termed L9A), with the two peptides containing the L16G substitution named L16G E20C and L16G E20C Y17H, denoting all substitutions from GCN4-pLI.

Peptide Synthesis. Peptide synthesis was typically performed on Fmoc-Arg(Pbf)-Wang resin using an Advanced ChemTech 348Ω automated synthesizer, with diisopropyl carbodiimide (DIC) and *N*-hydroxybenzotriazole (HOBt) in *N*-methylpyrrolidinone (NMP) for couplings, and 30% piperidine in NMP for deprotection. N-Termini of peptides were acetylated with 2:2:1 NMP/acetic anhydride/*N*,*N*-diisopropylethylamine (DIEA) solutions. Side chain protecting groups were Arg(Pbf), Ser(tBu), Lys(Boc), Glu(tBu), Asp(tBu), Tyr(tBu), Gln(Trt), Asn(Trt), Cys(Trt), and His(Trt). Cleavage

of peptides was typically effected with a 94:2.5:2.5:1 TFA/ethanedithiol/water/triisopropylsilane mixture for 4 h. Peptides were precipitated with ether (50 mL), centrifuged, and washed with ether. Following being dried in vacuo, peptides were purified on a C18 column (Vydac 218TP) eluting with a water/acetonitrile/TFA gradient, and lyophilized. Molecular weights of peptides were verified using a PerSeptive Biosystems Voyager DE MALDI-TOF[1] mass spectrometer.

Circular Dichroism Spectroscopy. Peptide stock solutions in water for CD spectroscopy were prepared at a concentration of 20 mg/mL and standardized by measurement of tyrosine absorbance. Typically, a 10 μL aliquot of stock solution was diluted with 1.0 mL of buffer [50 mM phosphate and 150 mM NaCl (pH 7.0)], and absorbance was measured at 280 nm. Measurements were taken in triplicate. The concentration was determined assuming $\epsilon_{280} = 1280\ M^{-1}\ cm^{-1}$. Peptide stock solutions were stored at −80 °C, and diluted to an appropriate concentration with buffer or water before use. CD thermal melts were recorded in stirred 0.5 cm path length cuvettes with 10 μM peptide in buffer [50 mM phosphate, 150 mM NaCl (pH 7.0), and 1 M guanidine hydrochloride]. Added dithiothreitol (0.5 mM) was included as a reducing agent for the peptides containing the E20C substitution. The temperature was increased in 2 °C intervals, with an equilibration time of 90 s, before the CD signal at 222 nm was recorded. The CD signal versus temperature was fit to a fourth-order polynomial over the melting transition, and the melting temperature (T_m) was calculated as the point at which the second derivative of this function was zero.

Size Exclusion Chromatography. Peptide stock solutions were prepared as described above for CD experiments. Size exclusion chromatography (SEC) was performed at room temprature on a Superdex 75 10/30 column eluted with buffer [50 mM phosphate and 150 mM NaCl (pH 7.0)] at a flow rate of 0.5 mL/min. The samples for calibration were bovine serum albumin (2.5 mg/mL, MW = 67 000), bovine erythrocyte carbonic anhydrase (2 mg/mL, MW = 29 000), horse skeletal muscle myoglobin (1 mg/mL, MW = 17 600), horse heart cytochrome *c* (1 mg/mL, MW = 12 384), aprotinin (2 mg/mL, MW = 6500), bovine oxidized insulin B chain (2 mg/mL, MW = 3496), and cyanocobalamin (1 mg/mL, MW = 1355). Aliquots (20 μL) of each of the calibrant solutions were mixed and injected. The elution volume was plotted against MW and fit using nonlinear regression with Mathematica. The peptide stock solutions in water were diluted with elution buffer to final concentrations of 250 μM, of which 50 μL was injected. Monitoring was carried out by ultraviolet (UV) absorption at 214 nm. Apparent aggregation states (N_{agg}) were calculated from the elution volume by first using the calibration plot to determine the apparent MW of the bundle and then dividing this value by the calculated MW of an individual peptide. A control peptide reported to form a coiled-coil trimer in solution (*14*) had an observed N_{agg} of 3.2.

[1] Abbreviations: CD, circular dichroism; SEC, size exclusion chromatography; ABA, acetamidobenzoic acid; MW, molecular weight; N_{agg}, apparent aggregation number; UV, ultraviolet; MALDI-TOF, matrix-assisted laser desorption ionization time-of-flight; SSRL, Stanford Synchrotron Radiation Laboratory; APS, Advanced Photon Source; SIR, single isomorphous replacement; VDW, van der Waals.

Crystallization and Data Collection. Peptide stock solutions for crystal growth were prepared at a concentration of approximately 20 mg/mL in 50 mM Tris-HCl buffer (pH 7.0 prior to addition of peptide) or in water alone. Stock solutions were filtered through a 0.22 μm membrane filter before use. The final concentration as measured by UV was typically ∼2 mM. Crystal screens were performed using Crystal Screen 2, Cryo Screen (Hampton Research), or Wizard II (Emerald Biostructures) kits. Hanging drop volumes of 1−2 μL of peptide stock with 0.1−1 μL of added buffer were used with buffer reservoir volumes of 0.5−1 mL. Peptide L16G E20C Y17H was crystallized by screening using an Innovadyne spotting robot, employed due to the difficulty of obtaining crystals for this peptide. Crystallization buffers consisted of 10% (w/v) PEG 6000 and 2 M NaCl with no cryoprotectant (peptides L9G, L9S, L9A, L9T, L9A+IB, L9G+IB, and L16G E20C); 10% (w/v) PEG 8000, 100 mM Tris (pH 7.0), and 200 mM $MgCl_2$ with glycerol and ethylene glycol as cryoprotectant (peptide L23G); 2.5 M NaCl, 100 mM NaOAc (pH 4.5), and 200 mM Li_2SO_4 with glycerol and ethylene glycol as cryoprotectant (peptides GCN4-pLI, L23S, I26G, I26A, I26S, and I26T); and 20% PEG 3350 and 200 mM KSCN (peptide L16G E20C Y17H). We subsequently found that the 10% (w/v) PEG 6000, 2 M NaCl buffer was sufficient for all peptides crystallized in the $P4_132$ lattice. The crystals from this condition displayed characteristic cubic or rhombododecahedral shapes, and exhibited no birefringence (characteristic of a cubic unit cell). The antiparallel peptide (L16G E20C Y17H) crystallized in the trigonal $P3_1$ space group.

Crystals were mounted on nylon loops, immersed in the cryoprotectant, and frozen at ∼100 K in the diffractometer cryostream. Data for L9G and L9G+IB crystals were collected at Stanford Sychrotron Radiation Laboratory (SSRL), and L16G E20C Y17H data were collected at Advanced Photon Source (APS) beamline GM/CA-CAT. Data for the remaining crystals were collected using MSC R-Axis IV or Mar345 image plate detectors [wavelength of 1.54 Å, $I(f',f'') = (-0.31,6.90)$]. Integration and scaling were carried out with CrystalClear (MSC) (*32*), Mosflm (*33*) and HKL2000 (*34*), and the CCP4 suite of programs (*35*, *36*). The initial structure determination was performed on a small cubic crystal (0.15 mm on an edge) of the L9G variant using experimental phases obtained from single isomorphous replacement (SIR) heavy atom phasing of xenon diffused into the crystal. The data were collected at SSRL beam line 9-1 (wavelength of 0.97 Å) using the SSRL pressure cell to pressurize the crystal for 3 min at 300 psi of xenon (*37*). A single ordered Xe atom was found to occupy the small cavity at the I26 position, and not the large cavity at the L9G site. This structure was subsequently used as an initial model to determine the remaining parallel structures via molecular replacement using Molrep (*35*). The structure of L16G E20C Y17H was determined with Phaser (*38*) using a truncated (residues 5−30) single strand from L16G E20C as a model for molecular replacement. Structural refinements were carried out using Refmac5 (*35*) and XtalView (*39*).

We took care to ensure that our space group assignment for the cubic crystals was correct. After scaling and averaging complete data in the maximal nonisomorphic subgroup $P2_13$ and performing molecular replacement and refinement, we did not observe improvement in R and R_{free} (while doubling

the number of fitted parameters). The iodine anomalous difference maps for the L9G+IB and L9A+IB complexes independently demonstrated 2-fold symmetry when the data were processed in $P2_13$. The systematic absences at $h00 = 0k0 = 00l \neq 4n$ for all structures also support the $P4_132$ assignment. The first three N-terminal residues and the last three C-terminal residues generally provided very weak electron density and proved to be difficult to fit in most structures. Residues that could not be fit [either manually or using ARP/warp (*40*)] were omitted from the structure, which is reflected in the higher R_{free} values in structures such as I26G. All peptides exhibit higher *B* factors toward the ends of the chain and lower *B* factors for central residues, particularly those in the hydrophobic core, which is likely because both termini of the tetramer are effectively free of crystal contacts in the $P4_132$ lattice.

Iodobenzene complexes were prepared by crystallizing peptides L9G and L9A by placing 2 μL of iodobenzene liquid (Aldrich) on top of the aqueous drop. Reflection data for L9G+IB were collected at SSRL beam line 11-1 [wavelength of 0.82 Å, $I(f',f'') = (-0.22,2.34)$]. A highly redundant data set was collected for L9G+IB (20-fold) to ensure observation of the anomalous signal from the iodine atom in iodobenzene. The L9A+IB crystal data set was not collected to such a high redundancy as that of L9G+IB because of the stronger anomalous scattering factor at the Cu Kα wavelength.

Superhelical parameters and cavity volumes were determined using FITCC (M. Sales, personal communication; http://ucxray.berkeley.edu/~mark/fitcc.html) and VOIDOO (*41*), respectively. On the basis of the 2.0 Å resolution data obtained for most crystals, we estimate errors in atomic positions of the refined structures to be ±0.2 Å, and the resulting errors for cavity volumes to be ~15%. The volume of iodobenzene was also calculated using VOIDOO. Root-mean-square (rms) deviations were calculated using the McLachlan algorithm (*42*) as implemented in ProFit (A. C. R. Martin, http://www.rfcgr.mrc.ac.uk/Registered/Help/profit/).

Table 2: Apparent Aggregation States, Thermal Denaturation Values, and Probe-Occupied Cavity Volumes for GCN4-pLI and Variants, along with Surface Areas and Volumes for Relevant Amino Acids

peptide	N_{agg}[a]	T_m (°C)[c]	cavity volume (Å^3)[e] 1.4 Å probe radius	cavity volume (Å^3)[e] 1.8 Å probe radius
GCN4-pLI	4.3	94[d]	20−40	0
L9G	4.1	64	tunnel[f]	220
L9G+IB	~	~	tunnel[f]	240
L9S	4.1	68	100	80
L9A	4.0	70	220	190
L9A+IB	~	~	tunnel[f]	210
L9T	4.0	95	~[g]	~[g]
L16G E20C	3.9	37	330	260
L16G E20C Y17H	3.7[b]	37	370	300
L23G	3.8	51	280	230
L23S	4.0	66	150	120
L23A	4.1	80	~[h]	~[h]
L23T	4.0	84	~[h]	~[h]
I26G	5.0	75	~[g]	~[g]
I26S	4.7	78	tunnel[f]	520
I26A	4.3	88	200	110
I26T	4.2	87	80	0

amino acid	side chain nonpolar surface area (*43*) (Å^2)	side chain volume (*37*) (Å^3)
Gly	47	~
Ala	86	26.3
Ser	56	30.4
Thr	90	56.2
Ile	155	101.1
Leu	164	100.8

[a] Apparent aggregation number as measured by SEC. Estimated errors are ±0.1. [b] Approximately 20% of the sample eluted with an N_{agg} of 3.0. [c] Thermal denaturation curves determined by CD in neutral solutions containing 1 M guanidinium hydrochloride. Estimated errors are ±2 °C. [d] Performed in 3 M guanidinium hydrochloride. [e] On the basis of the reported high-resolution values of ~2.0 Å, we estimate errors in cavity volume to be ~15%. [f] The cavity was not enclosed on all sides, creating a tunnel through the peptide assembly. [g] Electron density could not be modeled beyond the site of the cavity, preventing determination of the cavity volume. [h] Crystals were not obtained for this peptide.

RESULTS AND DISCUSSION

By replacing bulky hydrophobic residues with smaller residues in the buried core of a homotetrameric coiled coil, we hoped to create internal cavities (Figure 1). Terminal hydrophobic core *a* (sites 9 and 23) and *d* (site 26) heptad positions of the 33-residue GCN4-pLI were initially chosen as amino acid substitution sites, since we thought that making substitutions near the termini would likely leave much of the peptide's association energy intact and drive folding of the desired parallel tetrameric state. Variants containing single Gly, Ala, Ser, or Thr substitutions (chosen to sample a range of side chain sizes and polarities) at each of these three sites were thus prepared. The study was later expanded with two additional peptides, both containing an E20C substitution [which has recently been shown to switch the crystal structure of GCN4-pLI from parallel to antiparallel (*31*)] and an L16G substitution, to characterize internal cavities within tetramers adopting an antiparallel crystallographic configuration. In an antiparallel homotetramer, a large single cavity can be created only at the center of peptide (position 16), since the more terminal regions of the assembly juxtapose two N-terminal residues and two C-terminal residues. All peptides are named for their respective substitution, and sequences are listed in Table 1.

Solution Studies. Each peptide, with the exception of I26G and I26S, exhibited the expected tetrameric aggregation state at peptide concentrations of 250 μM in neutral phosphate-buffered aqueous solutions, and all peptides except L16G E20C Y17H eluted as single, sharp peaks from the size exclusion column, discrediting the possibility of multiple aggregation states in solution (Table 2). We attribute the larger N_{agg} values of I26G and I26S to C-terminal fraying which increases the apparent size of the aggregate. This explanation is supported by the crystallographic observation of C-terminal fray and disorder (described below) and is probably most pronounced at the I26 position since it is the most terminal of the four substitution sites. The L16G E20C Y17H peptide is predominantly tetrameric in solution, but a small proportion (roughly 20%) elutes with an N_{agg} of 3.0. This result demonstrates that hydrophobic core substitutions near the center of the assembly are more structurally perturbative than substitutions at the helix termini.

All peptides displayed circular dichroism (CD) spectra typical of α-helical coiled coils with minima at 222 and 208 nm. As shown in Table 2, thermal stabilities of the pLI

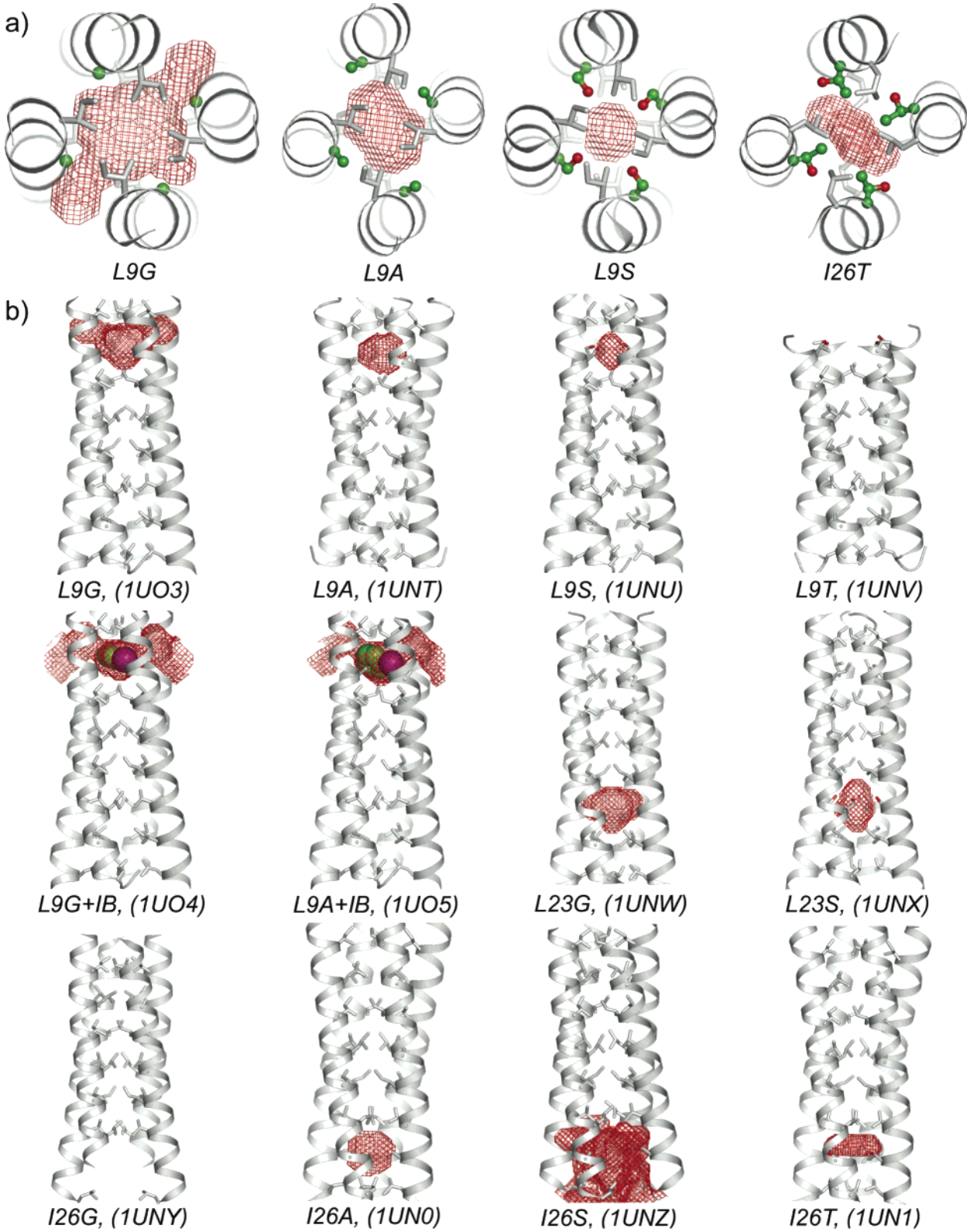

FIGURE 2: Crystal structures and cavities of GCN4-pLI variants. (a) Cross sections and (b) side views depicting red mesh surfaces for the calculated 1.4 Å radius probe-occupied cavities or tunnels. The substituted residues are shown using ball-and-stick representations, while other core residues are shown with sticks. VDW spheres are shown for iodobenzene. PDB entries are given in parentheses.

variants (10 μM peptide, pH 7.0 phosphate buffer containing 1 M guanidine hydrochloride) generally correlate with the nonpolar surface area of the substituted residue (*43*), where the more stable assemblies are those containing the more nonpolar amino acids (Table 2). An important consequence of this stability profile is that peptides containing larger cavities created by an Ala core substitution are more stable than the peptides containing smaller cavities created by Ser substitutions (see below for a discussion of cavity size). The core residues closer to the center of the assembly contribute more to the thermal stability of the bundle, accounting for the lower melting temperatures of the variants containing

Table 3: Data Collection and Refinement Statistics[a]

peptide	edge length (Å)	resolution (Å)	total no. of observations	no. of unique reflections	I/σ (average)	I/σ (outer)	R_{sym}	R	R_{free} (~5%)
$P4_132$									
GCN4-pLI	79.6	1.99	37 822	6330	6.8	1.6	0.064	0.242	0.286
L9G	79.2	1.91	85 641	6964	7.5	1.3	0.059	0.235	0.281
L9S	78.5	2.07	53 164	5435	17.0	3.1	0.030	0.231	0.270
L9A	78.4	2.07	34 573	5427	13.8	2.1	0.035	0.227	0.286
L9T	78.1	2.07	34 996	5363	9.1	1.6	0.055	0.230	0.290
L9G+IB	79.1	1.70	188 225	9782	5.5	2.0	0.080	0.225	0.257
L9A+IB	78.5	2.07	71 214	5435	14.6	3.2	0.030	0.260	0.280
L23G	78.5	2.30	50 281	4599	8.3	1.1	0.059	0.250	0.284
L23S	78.8	2.03	38 975	3607	3.4	1.7	0.140	0.249	0.314
I26G	79.3	2.30	57 910	4127	8.8	1.9	0.063	0.256	0.322
I26S	79.3	1.80	85 655	8233	7.1	1.0	0.066	0.259	0.312
I26A	79.3	2.40	45 238	3676	5.8	1.3	0.123	0.229	0.299
I26T	79.4	2.22	40 086	3283	7.5	1.9	0.094	0.259	0.312
L16G E20C	78.4	2.17	35 342	4747	5.7	1.9	0.078	0.269	0.292
$P3_1$									
L16G E20C Y17H	25.8, 25.8, 148.6	1.50	89 229	17250	25.7	4.7	0.068	0.238	0.276

[a] All data sets were >97% complete.

the substitution in the central L16 position relative to peptides with more terminal substitutions.

Crystal Structures. Here we describe the crystal structure of GCN4-pLI in a space group different from that originally reported (*14*) (Figure 1a), and report structures of 11 peptides in the parallel configuration and one peptide in the antiparallel configuration containing hydrophobic core substitutions (Figure 2 and Table 3). All crystals in which peptides adopted the parallel configuration were processed in the $P4_132$ space group, where the four-helix bundle is generated by a crystallographic 2-fold symmetry axis acting on the two-strand asymmetric unit, so that 12 four-helix bundles comprise the unit cell contents. Peptide L16G E20C Y17H was processed in the $P3_1$ space group, in which the asymmetric unit is an all-antiparallel coiled-coil tetramer. The observation of an antiparallel configuration for this peptide, which contains an E20C substitution, is consistent with our recent report describing crystallization of several pLI variants containing the E20C substitution in the antiparallel assembly (*31*). Somewhat unexpectedly, peptide L16G E20C adopted the parallel configuration and crystallized in the $P4_132$ space group. It is unlikely that the N-terminal acetamidobenzoic acid (ABA) moiety causes the change in configuration, since we have determined both parallel and antiparallel structures of GCN4-pLI variants containing this N-terminal group (*31*). Computational studies are underway to address these observed changes in configuration. Nonetheless, the two closely related peptides, both containing L16G substitutions but adopting different quaternary structures, illustrate that at least two cavities of different shapes and sizes can be engineered from identical core substitutions.

A number of differences are apparent between the GCN4-pLI tetramer in the $P4_132$ space group reported here relative to the originally reported structure in the $P2_12_12_1$ space group (*14*). Most notable is the crystallographic 2-fold symmetry axis along the helix axis in the $P4_132$ space group, which results in each four-helix bundle being generated from just two unique chains, rather than four. The Glu6−Arg1 interhelical salt bridge is not observed in most cases, possibly because the N-terminal Arg residue often cannot be resolved. Other ionic lattice interactions in the original structure appear to be largely retained in the variants reported here. The final two C-terminal residues are not reported in the original structure and could only sometimes be modeled in the structures presented here. An α-carbon superposition of the two tetrameric structures for residues 2−29 resulted in a root-mean-square (rms) deviation of 1.06 Å. Because the termini of the tetrameric peptide assembly are essentially free of crystal contacts in the $P4_132$ lattice, *B* factors increase from the center of the assembly to the termini.

Cavities. Coiled coils generally contain small internal cavities between the *a* and *d* layers. These cavities are competent for occupation by small guests, as evidenced by the xenon binding used for the initial structure determination of the peptides reported here. In GCN4-pLI, there are three such interlayer cavities ranging in volume from ~20 to 40 $Å^3$ (using a probe with a radius of 1.4 Å). Substituting single hydrophobic core residues with Gly, Ser, Ala, or Thr creates cavities that are much larger than these interlayer cavities since the tetrameric assembly juxtaposes the four substitutions sites, creating an entire level of vacancy within the aggregate. Cavity sizes are reported as probe-occupied volumes for probes with radii of 1.4 or 1.8 Å (representing a water molecule or a chloride ion, respectively) (Table 2).

The engineered cavities demonstrate a significant span of volumes and range from hydrophobic to moderately polar (Figure 2). In some cases, the internal cavities are not completely closed off from bulk solvent (using a 1.4 Å probe), generating tunnels through the interior of the peptide assemblies. As expected from individual side chain volumes (*44*) (Table 2), the observed cavity sizes are greatest for Gly substitutions, followed by Ala, Ser, and finally Thr. The I26S peptide deviates from this trend, containing a much larger cavity than the other Ser variants due to a pronounced C-terminal fray. While present within the L23G and the more polar I26S cavities, structured water molecules are somewhat surprisingly not observed within any of the other polar cavities. Although the L16G E20C Y17H and L16G E20C peptides contain the same core substitution, the peptides have cavities with different volumes and shapes because of their contrasting antiparallel and parallel configurations (Figure 3). In the antiparallel L16G E20C Y17H peptide, Ile19 and Cys20 pairs enclose the cavity on two sides, but this

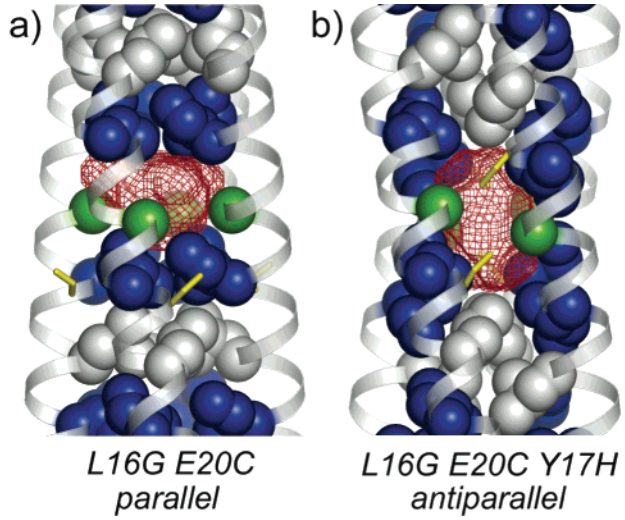

FIGURE 3: Crystal structures of L16G variants of GCN4-pLI. (a) L16G E20C adopts a parallel tetrameric configuration, creating a 330 Å^3 cavity (using a probe with a radius of 1.4 Å). Hydrophobic core *a* position Leu (blue) and *d* position Ile (gray) residues are shown with van der Waals (VDW) surfaces, as are α-carbons of the Gly16 residues (green). The Cys20 residues are shown as yellow sticks. (b) L16G E20C Y17H adopts an antiparallel tetrameric configuration, creating a vertically elongated 370 Å^3 cavity. The coloring is identical to that in panel a.

elongated cavity's volume is still greater than that in the parallel L16G E20C peptide. The cavities within the L16G peptides are the largest fully enclosed cavities using a 1.4 Å radius probe, although these peptides are also the least thermally stable.

Polar contacts are formed in the variants containing Ser or Thr core substitutions (*21*) that likely compensate somewhat for the destabilizing placement of polar groups in the hydrophobic core (Figure 4). On the basis of distance criteria (interatomic distances of <4 Å), each side chain hydroxyl group in the Ser and Thr variants forms backbone hydrogen bonds to the carbonyl oxygen of the *i* or *i* − 4 residue, where the *i* − 4 residue can be resolved (L9S, L23S, I26S, and I26T). In the L23S variant, one of the unique Ser residues forms a polar interaction with Glu22, thereby participating in an interhelical polar network (interatomic distances of 3.1−3.8 Å) among residues Glu22, His18, and Glu20 (Figure 4a). Along with the *i*, *i* − 4 hydrogen bond, the chain B Ser of I26S forms a backbone hydrogen bond with the *i*, *i* − 3 carbonyl, while the chain A Ser interacts with a structured water molecule bound inside the cavity (Figure 4b).

The polar side chains of the Ser and Thr variants pack differently depending on the heptad positioning of the substitution. In contrast to the Ser substitutions at *a* heptad positions (L9S and L23S) in which the side chains adopt the same rotamer and the hydroxyls are projected toward the center of the peptide assembly (Figure 4a), the *d* position Ser hydroxyls in I26S are skewed away from the cavity and the two unique side chains adopt different rotameric conformations (Figure 4b). Similarly for the Thr variants, the *d* position I26T hydroxyl groups projects away from the center of the peptide assembly such that the side chain methyl group is oriented toward the cavity. In the *a* position L9T variant, the hydroxyl groups are contrastingly projected toward the center of the cavity with the side chain methyl groups directed toward bulk solvent. As the closest hydroxyl groups

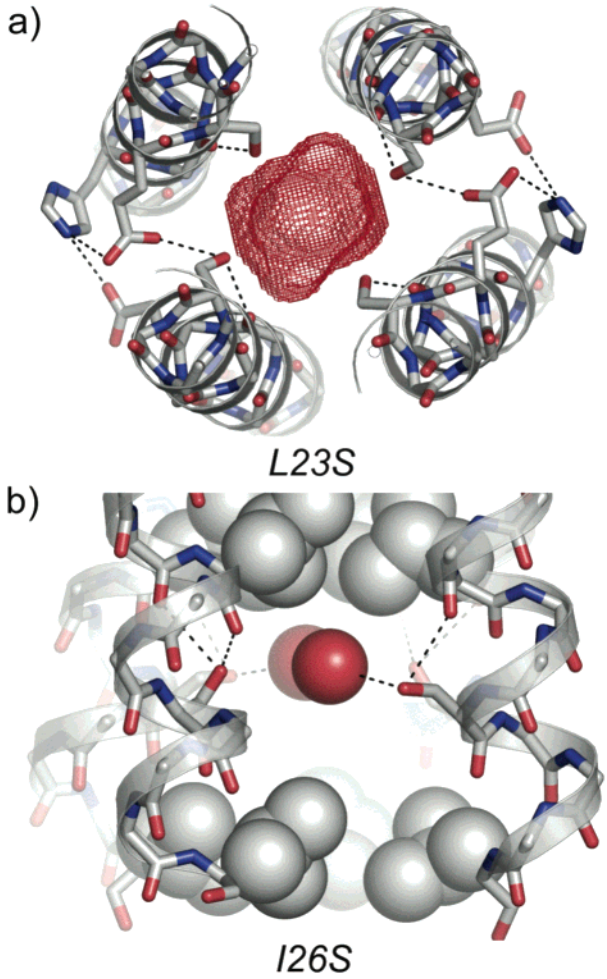

FIGURE 4: Electrostatic interactions in GCN4-pLI variants containing polar core substitutions. (a) Cross section of the L23S variant, illustrating polar contacts between the Ser23 hydroxyl groups and backbone or side chain atoms of adjacent residues. Sticks are shown for Ser23, Glu22, Glu20, and His18, and dashed black lines represent potential contacts. The 150 Å^3 cavity is colored red. (b) Side view of the I26S variant, depicting polar contacts between the Ser26 hydroxyl groups and backbone atoms or water molecules inside the cavity. Both unique Ser residues form at least two polar contacts (based on interatomic distances of >4 Å). VDW spheres are shown for water molecules (red) and hydrophobic core residues (gray), while sticks are shown for Ser26 and backbone atoms. Dashed black lines represent potential contacts.

in L9T are separated by 4.7 Å, these groups appear not to be forming polar contacts, and the presence of these four polar groups within the core might explain the observed lack of N-terminal electron density beyond this substitution site.

Iodobenzene Binding. We reasoned that a relatively small hydrophobic molecule might bind the more hydrophobic cavities formed by Gly or Ala substitutions, so we cocrystallized several of these peptides with iodobenzene. The presence of an iodine atom bound within the cavities of L9A and L9G was independently confirmed by the strong 5σ peak apparent at the same position in both the $|F_o| - |F_c|$ difference Fourier map (Figure 5) and the anomalous difference Fourier map for both peptides when crystallized in the presence of iodobenzene (L9A+IB and L9G+IB). There were no comparable peaks observed in any of the anomalous difference maps for any of the structures crystallized without iodobenzene. These results are consistent with an iodobenzene molecule bound inside the cavities of the

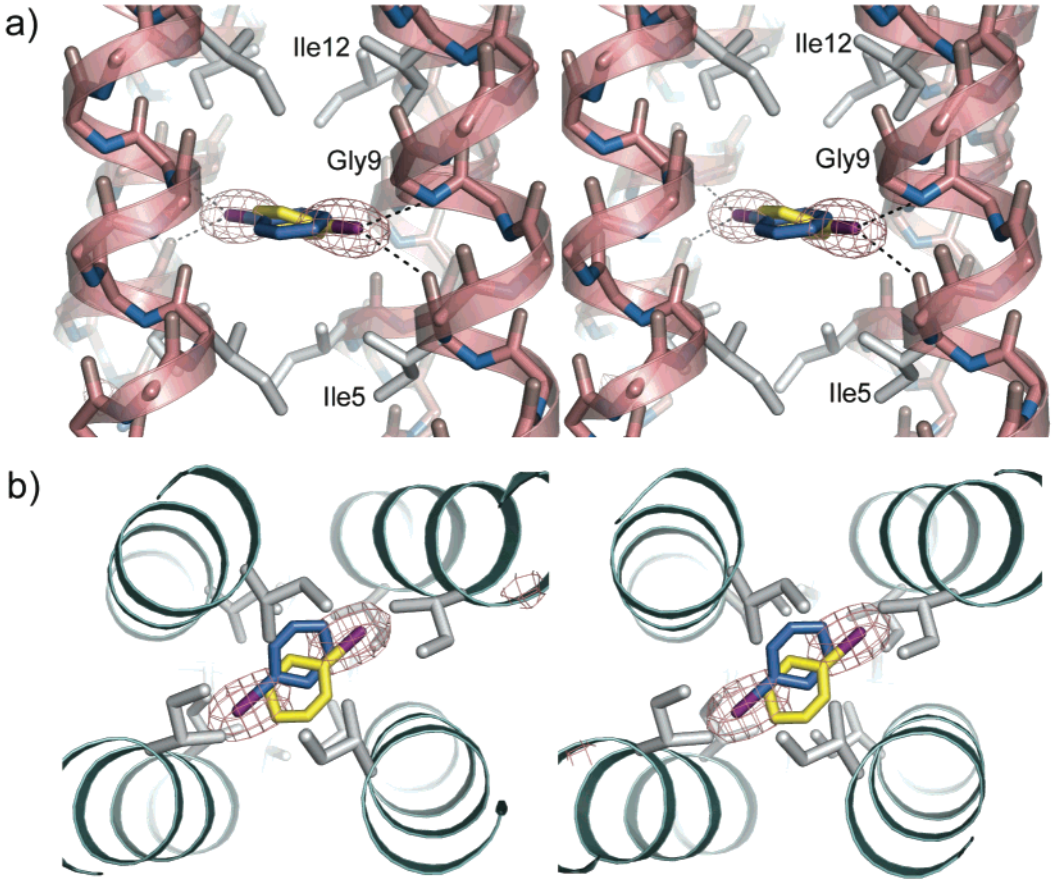

FIGURE 5: Stereoviews of iodobenzene bound within the hydrophobic cavity created in the L9G variant of GCN4-pLI. (a) Side view illustrating the potential polar contacts (dashed black lines) between the iodine atom and backbone nitrogen (interatomic distance of 3.9 Å) or carbonyl oxygen atoms (interatomic distance of 3.8 Å). The $F_o - F_c$ electron density (gray mesh, contoured at 4σ) indicates the positioning of the iodine atoms from the two symmetry-equivalent iodobenzene molecules (blue and yellow). Side chains of hydrophobic core residues are shown as gray sticks. (b) Top view of the iodobenzene-bound L9G using the same representations as panel a.

peptides, with a crystallographic C_2 axis running through the benzene ring (Figure 5 and Figure S1 of the Supporting Information). The $P4_132$ space group imposes two symmetry equivalent conformations of iodobenzene in the tetrameric coiled coil. While it is likely that the cavities described here will bind other molecules, the heavy atom anomalous signal made characterization of the iodobenzene complexes unequivocal.

The molecular volume of iodobenzene is 170 Å^3, which fills ~75% of the calculated cavities (1.8 Å radius probe) in L9G+IB and L9A+IB. However, these fractional occupation values are overestimates since there is a significant amount of void space not included in the calculated cavity when a 1.8 Å radius probe is used to measure the cavity. Although the cavities are not fully enclosed using a more reasonable 1.4 Å probe, we can estimate a more realistic cavity volume for L9G+IB using values from L16G E20C, L16G E20C Y17H, and L23G, all of which contain Leu → Gly mutations that are fully enclosed using both probe sizes. Applying the average difference in calculated volume for the two probe sizes for these three peptides (60 Å^3) to the L9G+IB cavity, we estimate a cavity volume for L9G+IB of 300 Å^3, which is ~60% occupied by the molecular volume of iodobenzene. A similar calculation for L9A+IB again results in an occupation value of ~60%. These fractional occupation values agree closely with the ideal encapsulation value of 55 ± 9% reported by Rebek and co-workers (*45*). The cavities within the L9A and L9G structures increase in volume by ~20 Å^3 when occupied by iodobenzene (Table 2). These volume increases result from greater N-terminal interhelical distances (described below), and likely take place to allow the most enthalpically favorable packing interactions between the host assembly and guest molecule. The plane of the iodobenzene aromatic ring is more tilted with respect to the long bundle axis in L9A+IB than in L9G+IB, which is likely due to the tighter packing in the smaller cavity.

The polarizable iodine atom of the bound iodobenzene is projected toward and potentially forms polar contacts with the backbone nitrogen of Gly9 (3.90 Å interatomic distance) and the backbone carbonyl oxygen of Ile5 (3.82 Å interatomic distance) (Figure 5a and Figure S1a of the Supporting Information), consistent with previous reports of polar interactions between halogen atoms and proteins (*46*, *47*). The L9G+IB and L9A+IB structures also contain new water molecules inside and near the periphery of the channel between the ligand and bulk solvent, which may be explained by the increased size of the cavity (Figure S1b of the Supporting Information). The side chains of Glu10 have distinctly different conformations in the unbound and bound forms. In the ligand-free L9G, both unique Glu10 residues form interhelical salt bridges with adjacent Lys8 residues and effectively occlude the empty cavity (Figure S1c of the Supporting Information). In contrast, these salt bridges are not present in the ligand-bound structure, which may be due

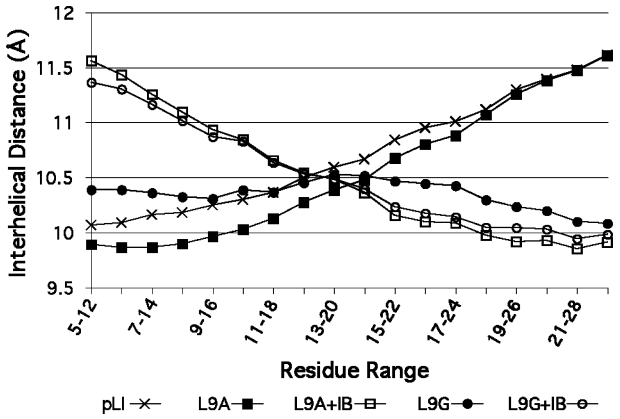

FIGURE 6: Interhelical distance profiles for GCN4-pLI (×), L9A (■), L9A+IB (□), L9G (●), and L9G+IB (○). The indicated heptads were used to determine the local interhelical distance values.

to, or which may contribute to, the increased interhelical distance and cavity size. In the free L9A structure, one of these Glu10−Lys8 interactions forms and is similarly absent in the bound structure. This conformational change can be clearly perceived in the "morph" movie (*48*) that has been generated between the bound and unbound forms (*49*).

Superhelical Parameters. Apart from the L9G and L9S peptides, GCN4-pLI and all variants that crystallized in the $P4_132$ space group display an increase in interhelical distance from the N-termini to the C-termini (Figure 6), as determined by calculating local supercoil parameters by fitting residues 5−29 in discrete bins of seven residues at a time (see the Supporting Information for further superhelical parameters). This drift in interhelical distance in not present in the originally reported GCN4-pLI structure, and may therefore result from effects imposed by the cubic lattice. The notable exceptions of L9G and L9S, located ∼25 Å from the C-termini, demonstrate that core substitutions can affect the overall structure at relatively long distances; these exceptions might result from local disorder or solvent accessibility at the N-termini leading to tighter compensatory packing near the C-termini for these peptides.

There is a substantial increase in the N-terminal interhelical distance for the L9G+IB and L9A+IB assemblies compared with their ligand-free forms (Figure 6). This increased interhelical distance results in an enlarged, more solvent-accessible cavity that presumably is better able to accommodate the bound iodobenzene guest. Although only two examples are presented here, interhelical distance profiles may thus be diagnostic of guest binding in coiled coils. Together, the observed changes in interhelical distance profile, increases in cavity volume, and rotamer alterations in solvent-exposed side chains for L9G+IB and L9A+IB suggest that induced fit binding events (*50*, *51*) must be taken into consideration when designing artificial receptors or enzymes. These conformational changes associated with ligand binding complicate the rational design aspects of peptide and protein engineering, but also make more likely the potential of binding several molecules with different shapes in the same host assembly.

CONCLUSION

In summary, we have characterized internal cavities of different sizes and polarities in a series of parallel and antiparallel coiled-coil tetramers and have shown that these cavities in some cases can bind an exogenous small molecule. The three-dimensional structures illustrate some of the varied surfaces that can be constructed in closely related peptides with very similar overall folds and may provide a basis for the future design of de novo helical proteins. This study was only possible because of the substantial plasticity of the hydrophobic core in the GCN4-pLI coiled-coil tetramer to substitution. Mixtures of peptides such as those reported here might be used for such purposes as the dynamic combinatorial formation of peptide-based receptors, and such heteromeric peptide assemblies containing nonsymmetric cavities may augment the scope of the system described here.

ACKNOWLEDGMENT

We thank the staff at SSRL and APS and Professors Peter Kuhn and Raymond C. Stevens for their generous assistance. Use of the Advanced Photon Source was supported by the U.S. Department of Energy, Office of Science, Office of Basic Energy Sciences, under Contract W-31-109-Eng-38.

SUPPORTING INFORMATION AVAILABLE

Morph movie illustrating observed conformational changes for L9G and L9A upon iodobenzene binding, Figure S1, and tabulated local superhelical parameters for each peptide. This material is available free of charge via the Internet at http://pubs.acs.org.

REFERENCES

1. Xu, J., Baase, W. A., Baldwin, E., and Matthews, B. W. (1998) The response of T4 lysozyme to large-to-small substitutions within the core and its relation to the hydrophobic effect, *Protein Sci. 7*, 158−177.
2. Guo, Z., Zhou, D., and Schultz, P. G. (2000) Designing small-molecule switches for protein−protein interactions, *Science 288*, 2042−2045.
3. Takano, K., Yamagata, Y., and Yutani, K. (2003) Buried water molecules contribute to the conformational stability of a protein, *Protein Eng. 16*, 5−9.
4. Machicado, C., Bueno, M., and Sancho, J. (2002) Predicting the structure of protein cavities created by mutation, *Protein Eng. 15*, 669−675.
5. Xu, J., Baase, W. A., Quillin, M. L., Baldwin, E. P., and Matthews, B. W. (2001) Structural and thermodynamic analysis of the binding of solvent at internal sites in T4 lysozyme, *Protein Sci. 10*, 1067−1078.
6. Quillin, M. L., Breyer, W. A., Griswold, I. J., and Matthews, B. W. (2000) Size versus Polarizability in Protein−Ligand Interactions: Binding of Noble Gases within Engineered Cavities in Phage T4 Lysozyme, *J. Mol. Biol. 302*, 955−977.
7. Mulder, F. A. A., Hon, B., Muhandiram, D. R., Dahlquist, F. W., and Kay, L. E. (2000) Flexibility and Ligand Exchange in a Buried Cavity Mutant of T4 Lysozyme Studied by Multinuclear NMR, *Biochemistry 39*, 12614−12622.
8. Vlassi, M., Cesareni, G., and Kokkinidis, M. (1999) A correlation between the loss of hydrophobic core packing interactions and protein stability, *J. Mol. Biol. 285*, 817−827.
9. Buckle, A. M., Cramer, P., and Fersht, A. R. (1996) Structural and Energetic Responses to Cavity-Creating Mutations in Hydrophobic Cores: Observation of a Buried Water Molecule and the Hydrophilic Nature of Such Hydrophobic Cavities, *Biochemistry 35*, 4298−4305.
10. Eriksson, A. E., Baase, W. A., Wozniak, J. A., and Matthews, B. W. (1992) A cavity-containing mutant of T4 lysozyme is stabilized by buried benzene, *Nature 355*, 371−373.
11. Penning, T. M., and Jez, J. M. (2001) Enzyme redesign, *Chem. Rev. 101*, 3027−3046.
12. Harris, J. L., and Craik, C. S. (1998) Engineering enzyme specificity, *Curr. Opin. Chem. Biol. 2*, 127−132.

13. Crick, F. H. C. (1953) The packing of α-helices: Simple coiled-coils, *Acta Crystallogr. 6*, 689−697.
14. Harbury, P. B., Zhang, T., Kim, P. S., and Alber, T. (1993) A switch between two-, three-, and four-stranded coiled coils in GCN4 leucine zipper mutants, *Science 262*, 1401−1407.
15. Horne, W. S., Yadav, M. K., Stout, C. D., and Ghadiri, M. R. (2004) Heterocyclic Peptide Backbone Modifications in an α-Helical Coiled Coil, *J. Am. Chem. Soc. 126*, 15366−15367.
16. Wilcoxen, K. M. (2002) Ph.D. Thesis, The Scripps Research Institute, La Jolla, CA.
17. Gonzalez, L., Jr., Woolfson, D. N., and Alber, T. (1996) Buried polar residues and structural specificity in the GCN4 leucine zipper, *Nat. Struct. Biol. 3*, 1011−1018.
18. Gonzalez, L., Jr., Brown, R. A., Richardson, D., and Alber, T. (1996) Crystal structures of a single coiled-coil peptide in two oligomeric states reveal the basis for structural polymorphism, *Nat. Struct. Biol. 3*, 1002−1010.
19. Gonzalez, L., Jr., Plecs, J. J., and Alber, T. (1996) An engineered allosteric switch in leucine-zipper oligomerization, *Nat. Struct. Biol. 3*, 510−515.
20. Holton, J., and Alber, T. (2004) Automated protein crystal structure determination using ELVES, *Proc. Natl. Acad. Sci. U.S.A. 101*, 1537−1542.
21. Akey, D. L., Malashkevich, V. N., and Kim, P. S. (2001) Buried Polar Residues in Coiled-Coil Interfaces, *Biochemistry 40*, 6352−6360.
22. Obataya, I., Sakamoto, S., Ueno, A., and Mihara, H. (2001) Design and synthesis of 3 α-helix peptides forming a cavity for a fluorescent ligand, *Biopolymers 59*, 65−71.
23. Johansson, J. S., Gibney, B. R., Rabanal, F., Reddy, K. S., and Dutton, P. L. (1998) A Designed Cavity in the Hydrophobic Core of a Four-α-Helix Bundle Improves Volatile Anesthetic Binding Affinity, *Biochemistry 37*, 1421−1429.
24. Johansson, J. S., Scharf, D., Davies, L. A., Reddy, K. S., and Eckenhoff, R. G. (2000) A designed four-α-helix bundle that binds the volatile general anesthetic halothane with high affinity, *Biophys. J. 78*, 982−993.
25. Manderson, G. A., Michalsky, S. J., and Johansson, J. S. (2003) Effect of Four-α-Helix Bundle Cavity Size on Volatile Anesthetic Binding Energetics, *Biochemistry 42*, 11203−11213.
26. Manderson, G. A., and Johansson, J. S. (2004) Towards a three-α-helix bundle protein that binds volatile general anesthetics, *Biopolymers 75*, 338−354.
27. Schnarr, N. A., and Kennan, A. J. (2004) Strand orientation by steric matching: A designed antiparallel coiled-coil trimer, *J. Am. Chem. Soc. 126*, 14447−14451.
28. Schnarr, N. A., and Kennan, A. J. (2002) Peptide Tic-Tac-Toe: Heterotrimeric Coiled-Coil Specificity from Steric Matching of Multiple Hydrophobic Side Chains, *J. Am. Chem. Soc. 124*, 9779−9783.
29. Monera, O. D., Zhou, N. E., Lavigne, P., Kay, C. M., and Hodges, R. S. (1996) Formation of parallel and antiparallel coiled-coils controlled by the relative positions of alanine residues in the hydrophobic core, *J. Biol. Chem. 271*, 3995−4001.
30. Monera, O. D., Sonnichsen, F. D., Hicks, L., Kay, C. M., and Hodges, R. S. (1996) The relative positions of alanine residues in the hydrophobic core control the formation of two-stranded or four-stranded α-helical coiled-coils, *Protein Eng. 9*, 353−363.
31. Yadav, M. K., Leman, L. J., Stout, C. D., and Ghadiri, M. R. (2005) Crystal Structure of an Antiparallel Homotetrameric Coiled-Coil, unpublished results.
32. Pflugrath, J. W. (1999) The finer things in X-ray diffraction data collection, *Acta Crystallogr. D55*, 1718−1725.
33. Leslie, A. G. W. (1992) Recent changes to the MOSFLM package for processing film and image plate data, *Joint CCP4/ESF-EAMCB Newsletter on Protein Crystallography*, No. 26, Daresbury Laboratory, Warrington, U.K.
34. Otwinowski, Z., and Minor, W. (1997) Processing of X-ray diffraction data collected in oscillation mode, *Methods Enzymol. 276*, 307−326.
35. Collaborative Computational Project No. 4 (1994) The CCP4 suite: Programs for protein crystallography, *Acta Crystallogr. D50*, 760−763.
36. Potterton, E., Briggs, P., Turkenburg, M., and Dodson, E. (2003) A graphical user interface to the CCP4 program suite, *Acta Crystallogr. D59*, 1131−1137.
37. Cohen, A., Ellis, P., Kresge, N., and Soltis, S. M. (2001) MAD phasing with krypton, *Acta Crystallogr. D57*, 233−238.
38. Storoni, L. C., McCoy, A. J., and Read, R. J. (2004) Likelihood-enhanced fast rotation functions, *Acta Crystallogr. D60*, 432−438.
39. McRee, D. E. (1999) XtalView/Xfit: A versatile program for manipulating atomic coordinates and electron density, *J. Struct. Biol. 125*, 156−165.
40. Perrakis, A., Morris, R., and Lamzin, V. S. (1999) Automated protein model building combined with iterative structure refinement, *Nat. Struct. Biol. 6*, 458−463.
41. Kleywegt, G. J., and Jones, T. A. (1994) Detection, delineation, measurement and display of cavities in macromolecular structures, *Acta Crystallogr. D50*, 178−185.
42. McLachlan, A. D. (1982) Rapid comparison of protein structures, *Acta Crystallogr. A38*, 871−873.
43. Karplus, P. A. (1997) Hydrophobicity regained, *Protein Sci. 6*, 1302−1307.
44. Harpaz, Y., Gerstein, M., and Chothia, C. (1994) Volume changes on protein folding, *Structure 2*, 641−649.
45. Mecozzi, S., and Rebek, J., Jr. (1998) The 55% solution: A formula for molecular recognition in the liquid state, *Chem.—Eur. J. 4*, 1016−1022.
46. Auffinger, P., Hays, F. A., Westhof, E., and Ho, P. S. (2004) Halogen bonds in biological molecules, *Proc. Natl. Acad. Sci. U.S.A. 101*, 16789−16794.
47. Ippolito, J. A., and Christianson, D. W. (1992) The contribution of halogen atoms to protein−ligand interactions, *Int. J. Biol. Macromol. 14*, 193−197.
48. Echols, N., Milburn, D., and Gerstein, M. (2003) MolMovDB: Analysis and visualization of conformational change and structural flexibility, *Nucleic Acids Res. 31*, 478−482.
49. See Supporting Information or MolMovDB ID 929950-12297, http://molmovdb.mbb.yale.edu/cgi-bin/morph.cgi?ID=929950-12297.
50. Koshland, D. E., Jr. (1994) The lock-and-key principle and the induced-fit theory, *Angew. Chem., Int. Ed. Engl. 33*, 2375−2378.
51. Davis, A. M., and Teague, S. J. (1999) Hydrogen bonding, hydrophobic interactions, and failure of the rigid receptor hypothesis, *Angew. Chem., Int. Ed. 38*, 736−749.

BI050742A